Available online at www.sciencedirect.com
ScienceDirect
Vision Research 48 (2008) 1107–1124
Vision Research
www.elsevier.com/locate/visres

Spatial properties of curvature-encoding mechanisms revealed through the shape-frequency and shape-amplitude after-effects

Elena Gheorghiu *, Frederick A.A. Kingdom

McGill Vision Research, Department of Ophthalmology, McGill University, 687 Pine Avenue W., Rm. H4-14, Montreal, Que., Canada H3A 1A1

Received 13 July 2007; received in revised form 18 January 2008

Abstract

The shape-frequency and shape-amplitude after-effects, or SFAE and SAAE, are phenomena in which adaptation to a sinusoidal-shaped contour results in a shift in, respectively, the perceived shape-frequency and perceived shape-amplitude of a test contour in a direction away from that of the adapting stimulus. Recent evidence shows that the SFAE and SAAE are mediated by mechanisms sensitive to curvature [Gheorghiu, E., & Kingdom, F. A. A. (2007a). The spatial feature underlying the shape-frequency and shape-amplitude after-effects. *Vision Research, 47*(6), 834–844]. Therefore we have used the SFAE and SAAE as a tool to study curvature processing. We examined whether curvature-encoding mechanisms are selective for (i) shape-phase, (ii) curvature polarity (or sign) and (iii) local orientation. We also investigated whether (iv) the two orthogonal dimensions of a curve, the sag and the cord, are encoded independently, and (v) whether curvature encoders are organized in an opponent manner. SFAEs/SAAEs were measured for adapting and test contours that differed or not in a given spatial property, the rationale being that if the after-effects were smaller when adaptor and test differed in a particular spatial property then curvature-encoding mechanisms must be selective for that spatial property. Our results reveal that SFAEs and SAAEs show (i) a degree of selectivity to curves that are mirror symmetric (in our stimuli half-cycle sine-wave contours in cosine (0/180 deg) shape-phase); (ii) a degree of selectivity to the sign or polarity of curvature; (iii) a degree of selectivity to local orientation; (iv) independent coding of the sag and the cord of the curve, and (v) no evidence for opponent-curvature coding. The results agree with neurophysiological studies showing that simple shape dimensions are encoded independently.

Keywords: Contour-shape; Curvature; Adaptation; After-effect; Opponent; Polarity

1. Introduction

Physiological and brain imaging studies have shown that contour shapes are processed at different stages in the visual cortex, from oriented line and edge detectors in V1 (Hubel & Wiesel, 1968), to curvature-sensitive detectors in V1 and V2 (Anzai, Peng, & van Essen, 2007; Dobbins, Zucker, & Cynader, 1987; Dobbins, Zucker, & Cynader, 1989; Hedge & van Essen, 2000), to parts-of-shape and curvature detectors in V4 (Connor, Brincat, & Pasupathy, 2007; Gallant, Braun, & Van Essen, 1993; Gallant, Connor, Rakshit, Lewis, & Van Essen, 1996; Pasupathy & Connor, 1999; Pasupathy & Connor, 2001; Pasupathy & Connor, 2002) and finally to whole-shape detectors in IT and LOC (Gross, 1992; Ito, Fujita, Tamura, & Tanaka, 1994; Missal, Vogels, Li, & Orban, 1999; Murray, Kersten, Olshausen, Schrater, & Woods, 2002; Tanaka, 1996). Psychophysical results are also consistent with multi-stage cortical processing of shape (Gheorghiu & Kingdom, 2007a; Habak, Wilkinson, Zahker, & Wilson, 2004; Keeble & Hess, 1999; Koenderink & Richards, 1988; Levi & Klein, 2000; Regan & Hamstra, 1992; Suzuki & Cavanagh, 1998; Wilkinson et al., 2000; Wilson, 1991; Wilson & Richards, 1989).

In this communication we provide new psychophysical evidence concerning the spatial properties of the mechanisms that code contour *curvature*. Curvature plays an important role in the representation and recognition of shapes. A variety of models have been proposed for curvature *detection and discrimination*. These include:

* Corresponding author.
E-mail address: elena.gheorghiu@mcgill.ca (E. Gheorghiu).

0042-6989/$ - see front matter © 2008 Elsevier Ltd. All rights reserved.
doi:10.1016/j.visres.2008.02.002

end-stopped V1 cells (Dobbins et al., 1987; Dobbins et al., 1989); linear comparisons of 1st-stage orientation-selective filters (Kramer & Fahle, 1996; Tyler, 1973; Wilson, 1985; Wilson & Richards, 1989; Wilson & Richards, 1992); multiplicative combinations of 1st-stage orientation-selective filters (Poirier & Wilson, 2006; Zetzsche & Barth, 1990); comparisons of 1st-stage positional information (Watt & Andrews, 1982), perhaps via oriented 2nd-stage filters (Prins, Kingdom, & Hayes, 2007), and linear filters with a 2×3 matrix of receptive field sub-regions (Koenderink & Richards, 1988; Koenderink & van Doorn, 1982; Koenderink & van Doorn, 1987; Whittaker & McGraw, 1998).

It is important to bear in mind that in order to detect a curve versus a straight line, or to discriminate two curves, the visual system might only need to use a minimum amount of neural machinery, e.g. an end-stopped cell, or a pair of orientation-selective units separated in space. In the case of the latter mechanism, the visual system need only compare the outputs of a single orientation-selective unit positioned at different locations along the curve, or a pair of units with different orientation tunings (Wilson & Richards, 1989). Such a mechanism requires no a priori knowledge of the curve to be processed (Wilson & Richards, 1989).

On the other hand to represent or encode curvature as an independent feature dimension, the visual system presumably requires something more elaborate: an analysis of the distribution of responses from detectors tuned to different curvatures, with each curvature detector constructed from a number of oriented sub-units collinearly arranged in a curve-shape (Gheorghiu & Kingdom, 2007a; Kingdom & Gheorghiu, 2007). Indeed neurophysiological studies (Pasupathy & Connor, 2001; Pasupathy & Connor, 2002) have shown that V4 neurons encode shape in terms of combinations of local features that include curvature.

The mechanism by which curves are encoded as opposed to detected or discriminated is arguably best understood through studies of curvature appearance (Ben-Shahar & Zucker, 2004; Gheorghiu & Kingdom, 2007a; Gheorghiu & Kingdom, 2007b), precisely because the perceived curvature of a line will be signaled via the population response of curvature detectors, just as perceived orientation is signaled via the population response of orientation-selective detectors. An important class of appearance-based psychophysical tools are after-effects, and we have recently used two contour-shape after-effects, the shape-frequency and shape-amplitude after-effects, or SFAE and SAAE, to study both contour-shape and texture-shape encoding (Gheorghiu & Kingdom, 2006; Gheorghiu & Kingdom, 2007a; Gheorghiu & Kingdom, 2007b; Kingdom & Gheorghiu, 2007; Kingdom & Prins, 2005a; Kingdom & Prins, 2005b). The SFAE and SAAE are the perceived shifts in, respectively, the shape-frequency and shape-amplitude of a sinusoidal test contour following adaptation to a sinusoidal contour of slightly different shape-frequency/amplitude. As with other spatial after-effects such as the tilt and luminance spatial-frequency after-effects, the perceived shifts in the SFAE and SAAE are always in a direction away from that of the adaptation stimulus (Gheorghiu & Kingdom, 2007a). Gheorghiu and Kingdom (2007a) showed that the SFAE and SAAE are most likely mediated by mechanisms sensitive to *local curvature*, rather than to either local orientation or global shape-frequency/amplitude. Although Suzuki and Cavanagh (1998) also found evidence of adaptation to curvature, in their case extending across space to retinal areas that had not been adapted, their use of static stimuli makes it hard to rule out an influence of orientation adaptation, since Roach, Webb, and Mcgraw (2007) have recently showed that the tilt after-effect can also extend to un-adapted spatial locations. Therefore to our knowledge, the SFAE and SAAE are the first examples of curvature after-effects that are not dependent on adaptor shape-phase and which have been shown not to result from local orientation adaptation (Gheorghiu & Kingdom, 2007a).

Readers can experience the SFAE and the SAAE with quasi-half-wave-rectified sinusoidal-shaped contours (i.e. half-wave rectified sinusoidal-contours missing the d.c. part of contour) in Fig. 1a and b by first moving their eyes back and forth along the horizontal markers on the left for about a minute, and then transferring their gaze to the central spot on the right. The two test contours, which are identical, should appear different in shape-frequency or shape-amplitude. Both after-effects survive shape-phase randomization during adaptation, as can be experienced in the non-static, full-sinusoidal adaptor versions at http://www.mvr.mcgill.ca/Fred/research.htm#contourShapePerception.

Recently we investigated both photometric (luminance and chromatic) and geometric properties of the SFAE and SAAE (Gheorghiu & Kingdom, 2006; Gheorghiu & Kingdom, 2007a; Gheorghiu & Kingdom, 2007b). With regard to *photometric* properties we demonstrated that SFAEs and SAAEs revealed selectivity to luminance contrast-polarity, luminance scale, color direction and color-contrast-polarity (Gheorghiu & Kingdom, 2006; Gheorghiu & Kingdom, 2007b). The one exception was that the SFAE showed little selectivity along the luminance-chromaticity dimension (Gheorghiu & Kingdom, 2007b). Gheorghiu and Kingdom (2006)'s study of the SFAE also showed that edge shape encoding mechanisms give greater weight to fine compared to coarse luminance scales. With regard to *geometric* properties we showed that SFAEs and SAAEs did not result from adaptation to either local orientation, average unsigned curvature, periodicity/density (SFAE only), shape-amplitude (SAAE only) or global shape. Instead, the after-effects resulted from adaptation to local curvature (Gheorghiu & Kingdom, 2007a). In addition, we have shown evidence for multiplication of first-stage orientation-selective inputs for curvature-encoding (Kingdom & Gheorghiu, 2007).

The present study is motivated by certain recent findings/models concerning shape processing, which we now discuss. First, studies of shape processing have shown that different dimensions of shapes, such as convexity vs.

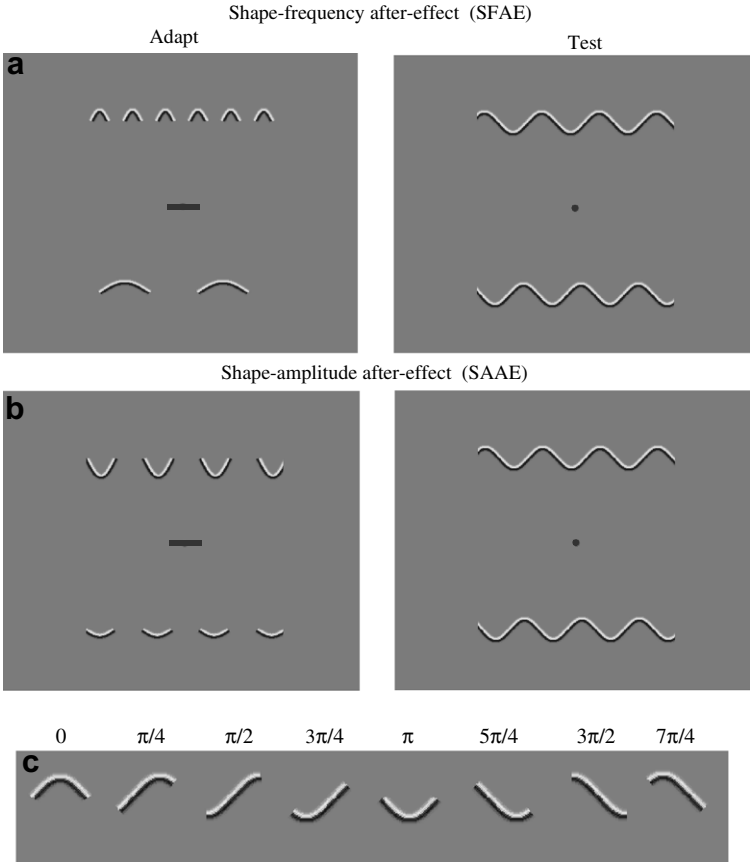

Fig. 1. Stimuli used in the experiments. One can experience (a) the shape-frequency after-effect (SFAE) and (b) the shape-amplitude after-effect (SAAE) by moving one's eyes back and forth along the markers located midway between the pair of adapting contours (left) for about 90s, and then shifting one's gaze to the middle of the test contours (right). (c) Experiment 1: a single segment of the adaptor in different shape-phases.

concavity, or curvature and tapering vs. aspect ratio, are encoded independently (Arguin & Saumier, 2000; Kayaert, Biederman, Op de Beeck, & Vogels, 2005; Op de Beeck, Wagemans, & Vogels, 2001). Several studies have shown that positive and negative curvatures play a different role in shape representation (Hoffman & Richards, 1984; Koenderink & van Doorn, 1982), and that there are perceptual asymmetries between positive and negative curvatures in various tasks and contexts such as change detection (Barenholtz, Cohen, Feldman, & Singh, 2003; Cohen, Barenholtz, Singh, & Feldman 2005), visual search (Hulleman, te Winkel, & Boselie, 2000; Xu & Singh, 2002) and localization (Bertamini, 2001). This has motivated us to consider whether curvature-encoding mechanisms are selective for curvature polarity.

Second, Gheorghiu and Kingdom (2007a) found that both SFAEs and SAAEs reached a maximum when the test contour was gated down to just half a cycle of a sinusoid centered on the peak or trough, i.e. ± cosine shape-phase. This raises the possibility that curvature-encoding mechanisms might be shape-phase tuned. However no detailed examination of curvature shape-phase tuning has to our knowledge been conducted, and therefore we have examined the selectivity of curvature-encoding mechanisms to shape-phase.

Third, Habak et al. (2004) found that radial-frequency patterns were masked equally by contours whose local orientations were either co-aligned or orthogonally aligned to the direction of the contour. This suggests a lack of selectivity to local orientation. However, Habak et al. measured detection thresholds and as we have argued above this may not necessarily reveal how curvature is represented. Therefore we have examined the selectivity of curvature-encoding mechanisms to local orientation.

Fourth, Gheorghiu and Kingdom (2007a) provided preliminary evidence suggesting that the SFAE and SAAE are separable after-effects, consistent with the idea that the sag and cord of a curve are encoded separately. They found that adaptation to shape-frequency had no effect on perceived shape-amplitude, and vice-versa. However, Gheorghiu and Kingdom (2007a) only tested one adaptor/test combination, and so the generality of the result has yet to be established. To this end we have tested whether the cord and sag of a curve are independently encoded over a range of adaptor/test combinations.

Fifth, Poirier and Wilson (2006), in their model of radial-frequency pattern detection, suggested that curvature detectors are organized in an opponent manner, as illustrated in Fig. 7a. However, although Poirier and Wilson showed that curvature-opponency was consistent with

their data on radial-frequency pattern detection, no direct evidence for curvature-opponency was provided, and to our knowledge none elsewhere exists. Therefore we have tested whether curvature-encoding mechanisms are organized in an opponent manner.

To summarize: We have used the SFAE and SAAE to answer the following questions. Are curvature-encoding mechanisms (1) selective for curves that are mirror-symmetric, that is in cosine phase, (2) selective for curvature polarity, (3) selective for local orientation, (4) selective for the curve's sag and cord, and (5) organized in an opponent manner?

2. General methods

2.1. Observers

Three subjects participated in the study. The two authors (E.G. and F.K.) participated in all experiments and one naive observer (A.Y.) participated in Experiment 1. All subjects had normal or corrected-to-normal visual acuity.

2.2. Stimuli

The stimuli were generated by a VSG2/5 video-graphics card (Cambridge Research Systems) with 12 bits contrast resolution, presented on a calibrated, gamma-corrected Sony Trinitron monitor, running at 120 Hz frame rate and with a spatial resolution of 1024×768 pixels. The mean luminance of the monitor was 42 cd/m^2.Example stimuli are shown in Fig. 1a and b. Adaptation and test stimuli consisted of pairs of either full sine-wave-shaped contours or half-wave-rectified sine-wave-shaped contours missing the 'd.c.', part of the contour, except in Experiment 3 in which only one adaptor was used. The mathematical equations used to construct these contours are given in the Appendix. Unless otherwise stated, the adaptor pair for the SFAE consisted of contours with a shape-amplitude of 0.43 deg and shape frequencies of 0.25 and 0.75 c/deg, giving a geometric mean shape-frequency of 0.43 c/deg. For the SAAE, the shape-frequency of the adaptor pair was 0.43 c/deg, while the shape-amplitudes were 0.25 and 0.75 deg, giving a geometric mean shape-amplitude of 0.43 deg. The two adaptors and tests were presented in the center of the monitor 3.5 deg above and below the fixation marker. The cross-sectional luminance profile of the contours was odd-symmetric and was generated according to a first derivative of a Gaussian function:

$$L(d) = L_{\text{mean}} \pm L_{\text{mean}} \cdot C \cdot \exp(0.5) \cdot (d/\sigma) \cdot \exp[-(d^2)/(2\sigma^2)] \quad (1)$$

where d is the distance from the midpoint of the contour's luminance profile along a line perpendicular to the tangent, L_{mean} is the mean luminance of 42 cd/m^2, C contrast of 0.5 and σ the space-constant of 0.044 deg. The $\pm$ sign determined the luminance polarity of the contour. Our contours were designed to have a constant cross-sectional width, and the method used to achieve this is described in Gheorghiu and Kingdom (2006).

2.3. Procedure

Each session began with an initial adaptation period of 90 s, followed by a repeated test of 0.5 s duration interspersed with top-up adaptation periods of 2.5 s. During the adaptation period, the shape-phase (ρ) of the contour (see Appendix) was randomly changed every 0.5 s in order to prevent the formation of afterimages and to minimize any effects of local orientation adaptation. The presentation of the test contour was signaled by a tone. The shape-phase (ρ) of the test contour was also randomly assigned in every test period. The display was viewed in a dimly lit room at a viewing distance of 100 cm. Subjects were required to fixate on the marker placed between each pair of contours for the entire session. A head and chin rest helped to minimize head movements.

A staircase method was used to estimate the PSE. For the SFAE the geometric mean shape-frequency of the two test contours was held constant at 0.43 c/deg while the computer varied the relative shape-frequencies of the two tests in accordance with the subject's response. At the start of the test period the ratio of the two test shape-frequencies was set to a random number between 0.33 and 3. On each trial subjects indicated via a button press whether the upper or lower test contour had the higher perceived shape-frequency. The computer then altered the ratio of test shape-frequencies by a factor of 1.06 for the first five trials and 1.015 thereafter, in a direction opposite to that of the response, i.e. towards the PSE. The session was terminated after 25 trials. In order that the total amount of adaptation for each condition was the same, we used a staircase method that was terminated after a fixed number (25) of trials, rather than a fixed number of reversals. We found in pilot studies that 25 trials were in general sufficient to produce a convergence that was stable over the last 20 trials. The shape-frequency ratio at the PSE was calculated as the geometric mean shape-frequency ratio of the tests adapted, respectively, by the lower and higher shape-frequency adaptors, averaged across the last 20 trials. The geometric rather than arithmetic mean is the appropriate way to average ratios (e.g. if one experiment yields a ratio of 10,000 and the other 0.0001, the arithmetic mean misleadingly gives an average ratio near 5000, whereas the geometric mean accurately gives a ratio of 1). Six measurements were made for each condition, three in which the upper adaptor had the higher shape-frequency and three in which the lower adaptor had the higher shape-frequency.

In addition we measured for each condition the shape-frequency ratio at the PSE in the absence of the adapting stimulus: the no-adaptor condition. To obtain an estimate of the size of the SFAE we calculated the difference between the logarithm of the with-adaptor shape-frequency ratio at the PSE and the mean logarithm of the no-adaptor shape-frequency ratio at the PSE, for each with-adaptor measurement. We then calculated the mean and standard error of these differences across measurements and these are the values shown in the graphs.

The procedure for measuring the SAAE followed the same principle as for the SFAE. The computer varied the relative shape-amplitudes of the two tests in accordance with the subject's response, while the geometric mean shape-amplitude of the two test contours was held constant at 0.43 deg.

3. Experiments and results

3.1. Experiment 1: Shape-phase

In this experiment we investigated whether curvature encoders are tuned for shape-phase. To do so, we used quasi-half-wave-rectified sine-wave-shaped contour adaptors and full sine-wave-shaped contour tests (see Fig. 1). We ask whether there is an optimal shape-phase of the component adaptor fragments for eliciting the SFAE and SAAE in full-sinusoidal test contours. The use of full sinusoidal test contours ensured that the subjects' *judgments* would not be influenced by shape-phase. In other words use of the same 'ruler' (full sinusoidal test contours) allowed valid comparisons across adaptor shape-phase. The mathematical equations used to construct full sine-wave-shaped contours and quasi-half-wave rectified sine-wave-shaped contours of various (φ) are given in the Appendix. There were eight adaptor shape-phases (φ): 0, $\pi/4$, $\pi/2$, $3\pi/4\pi$, $5\pi/4$, $3\pi/2$ and $7\pi/4$. Fig. 1a and b left shows examples of the 0 and 180 shape-phase adaptor con-

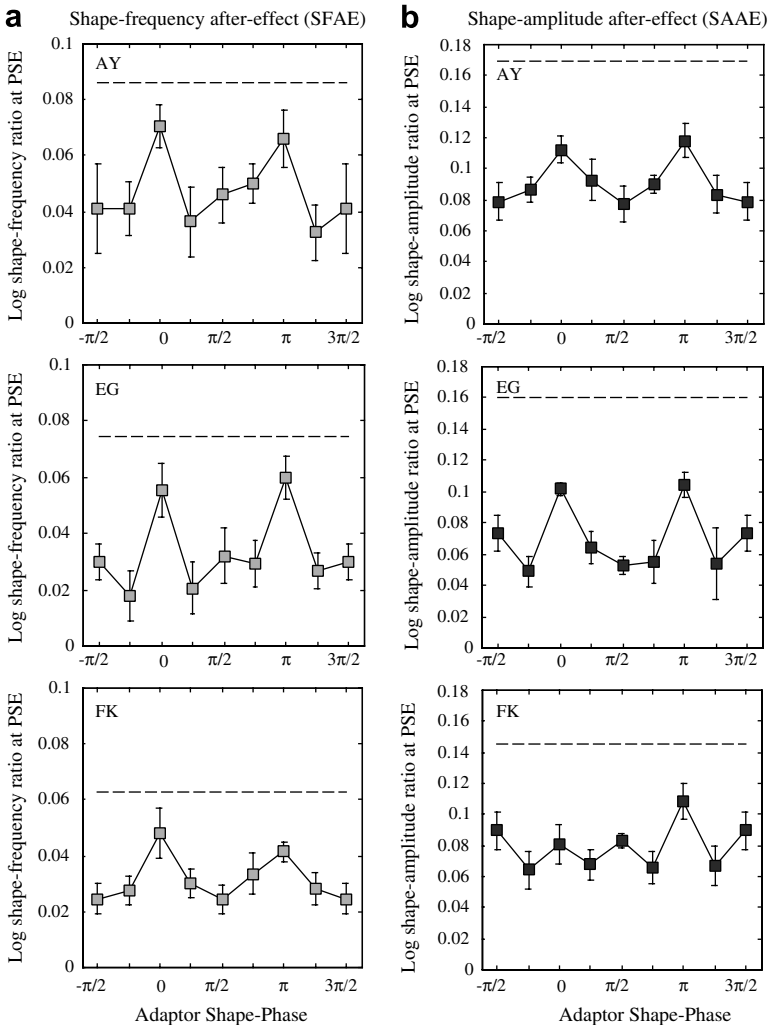

Fig. 2. Results for Experiment 1: (a) SFAEs (light gray symbols) and (b) SAAEs (black symbols) as a function of adaptor shape-phase. The dashed lines indicate the after-effects obtained with full sine-wave adaptors and tests.

ditions, while Fig. 1c shows single segments of all the adaptor shape-phase conditions. Note that during the adaptation period the phase (ρ) of the underlying waveform was randomly changed every 0.5 s, even though the shape-phase (φ) of the component fragments was fixed (see Appendix, Eq. (AI.3)). Thus for example in the condition shown in Fig. 1a, the subject would always see about 6 equally spaced half-cycle cosine-phase fragments, but the absolute position of a given fragment would change every 0.5 sec. We also measured the SFAE and SAAE with full sine-wave adaptors.

Fig. 2a shows SFAEs (light gray symbols) and Fig. 2b SAAEs (black symbols) as a function of adaptor shape-phase. The dashed lines indicate the after-effects obtained with full sine-wave adaptors. The after-effects obtained with quasi-half-wave-rectified adaptors are smaller that those obtained with full sine-wave adaptors, we assume because the energy of a continuous contour is greater than that of a fragmented one.

The results show that both after-effects reach a maximum when the half-cycle adapting fragments have shape-phases $\varphi = 0$ and $\varphi = \pi$, although sizeable after-effects are obtained with other shape-phases. The one exception was subject F.K.'s SAAE results (Fig. 2b, lower panel) where only one peak is present at +cosine shape-phase ($\varphi = \pi$). Overall, the results indicate that 0 and π (±cosine phase) are the optimum shape-phases for eliciting SFAEs and SAAEs.

One might think that the after-effects were largest at ±cosine phase and smallest at ±sine phase because these represented the two extremes in average unsigned curvature. However this cannot be the case because our ±cosine and ±sine phase fragments had the same averaged unsigned curvature.[1]

[1] To understand why the average unsigned curvature of a half-cycle sine and half-cycle cosine fragment is the same, consider dividing the waveform into three consecutive quarter-cycle fragments between π/2 and π. The average unsigned curvature of each of these three fragments will be the same on grounds of symmetry. Therefore any two of these fragments, whether combined to form a half-cycle sine, or half-cycle cosine fragment, will also have the same average unsigned curvature.

3.2. Experiment 2: Curvature polarity

In this experiment we investigated whether curvature-encoding mechanisms are *selective* for curvature polarity, or sign. To do this we compared the size of the after-effect for adaptors and tests that had the same curvature polarity with adaptors and tests that had a different curvature polarity. Hence unlike in the previous experiment, in which all the tests were full sinusoidal contours, the tests here were necessarily varied along the same dimension as the adaptors. Adaptor and test contours were constructed from quasi-half-wave-rectified, ±cosine fragments. Examples are shown in Fig. 3a–b. There were two conditions: (a) adaptor and test of the same curvature-polarity, either

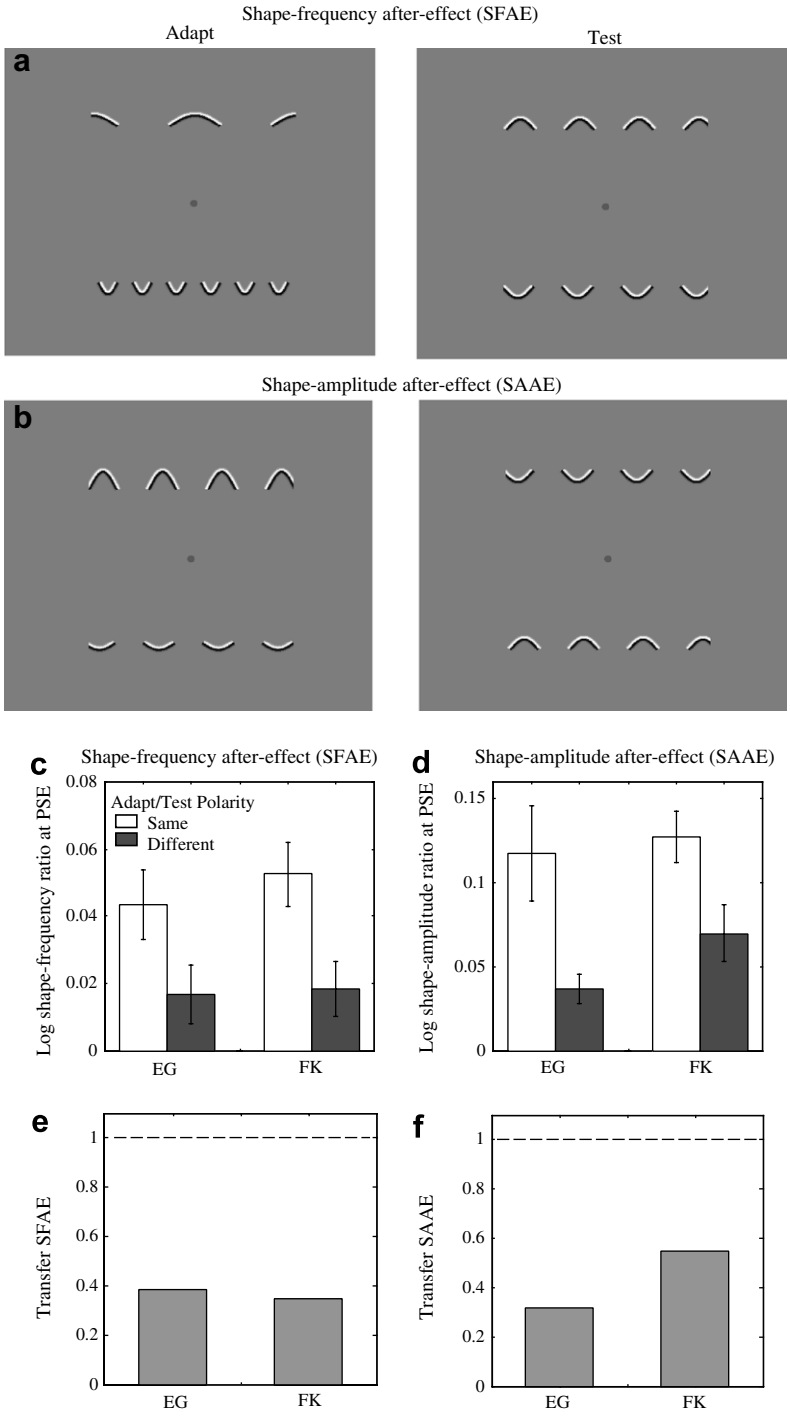

Fig. 3. (a–b) Stimuli used in Experiment 2: quasi-half-wave-rectified sinusoidal-shaped contours of positive and negative curvatures. (c–f) Results for Experiment 2: (c) SFAEs and (d) SAAEs for same (white bars) and different (gray bars) adaptor-test curvature-polarity conditions. (e) Transfer SFAE and (f) transfer SAAE between adaptor and test of different curvature-polarity. The value of 1 (dashed-line) indicates complete transfer whereas a value less than 1 indicates partial transfer.

positive or negative, and (b) adaptor and test of different curvature-polarity, that is, positive adaptor/negative test, and negative adaptor/positive test. Note that positive and negative curves were centered on a horizontal line that ran through the mid-point of each curve, i.e. positioned in the same vertical retinal locations and not in different vertical retinal locations as in the case of a full sine-wave contour.

Fig. 3 shows (c) SFAEs and (d) SAAEs for same (white bars) and different (dark gray bars) adaptor-test curvature-polarity conditions. The results show that the SFAEs and SAAEs are significantly reduced when adaptor and test contours are of different curvature polarity. In order to compare the reduction in the size of the after-effect between observers, we calculated the magnitude of transfer of after-effect we calculated the magnitude of transfer of after-effect, defined as the after-effect obtained with opposite curvature-polarity divided by the after-effect obtained with same curvature-polarity. Fig. 3e and f shows the transfer for both the SFAE and SAAE. The value of 1 (dashed-line) indicates complete transfer whereas a value less than 1 indicates partial transfer. Fig. 3e–f shows that both after-effects transfer only partially between different curvature-polarities (on average, 37% for SFAE and 44% for SAAE). These results indicate that SFAEs and SAAEs show a degree of selectivity to local curvature-polarity.

To test whether the after-effects are significantly larger for the same versus different curvature-polarity conditions we performed a two-way ANOVA (analysis of variance) with Sign (positive vs. negative) and Combination (same vs. different curvature polarity) as factors, on both the SFAE and SAAE data, for each subject. The main effect of Combination was significant [for SFAE: $F(1,1) = 15.96$, $p < 0.05$ for F.K.; $F(1,1) = 6.64$, $p < 0.05$ for E.G.; for SAAE: $F(1,1) = 11.83$, $p < 0.05$ for F.K.; $F(1,1) = 14.88$, $p < 0.05$, for E.G.]. The effect of Sign was not significant [for SFAE: $F(1,11) = 1.78$, $p > 0.01$ for F.K.; $F(1,11) = 0.72$, $p > 0.01$ for E.G.; for SAAE: $F(1,11) = 1.22$, $p > 0.01$ for F.K.; $F(1,11) = 0.99$, $p > 0.01$ for E.G.]. In addition, we performed a two-way ANOVA to test whether the different curvature-polarity conditions (gray bars) were significantly different from zero, i.e. from the non-adapted condition. They were significantly different [for SFAE: $F(1,1) = 15.7$, $p < 0.05$ for F.K.; $F(1,1) = 33.83$, $p < 0.05$ for E.G.; for SAAE: $F(1,1) = 16.71$, $p < 0.05$ for F.K.; $F(1,1) = 8.07$, $p < 0.05$ for E.G.].

3.3. Experiment 3: Sag vs. cord

Here we investigate whether the two principle axes of a symmetric curve, the sag and cord, are separately adaptable. We used quasi-half-wave-rectified sinusoidal-shaped contours and a single-adaptor method. This method differs from the one described in Sections 2.2 and 2.3 in that a single rather than a pair of adaptors was used. The single-adaptor method is similar to that employed by Gheorghiu and Kingdom (2007a). The adaptor was presented either above or below fixation, and the test was presented in the same location as the adaptor (see Fig. 4a). The comparison contour, which was adjusted during the test period to obtain the PSE, was presented in the other visual hemifield to that of the test. We used two adaptor conditions: (i) different shape-frequencies but same shape-amplitudes (0.5 deg)—the *adaptation-to-shape-frequency* condition, and (ii) different shape-amplitudes but same shape-frequencies (0.5 c/deg)—the *adaptation-to-shape-amplitude* condition (see Fig. 4a).

For the adaptation-to-shape-frequency condition, the adaptor, test and comparison contours all had shape-amplitudes of 0.5 deg. The test was fixed in shape-frequency at 0.5 c/deg, and the adaptor was set to one of ten shape frequencies: 0, 0.125, 0.177, 0.25, 0.354, 0.5, 0.707, 1, 1.414 and 2 c/deg. For the adaptation-to-shape-amplitude condition, the adaptor, test and comparison all had shape-frequencies of 0.5 c/deg. The test was set to a shape-amplitude of 0.5 deg, and the adaptor to one of ten shape-amplitudes: 0, 0.125, 0.177, 0.25, 0.354, 0.5, 0.707, 1, 1.414 and 2 deg. An example contour adaptor is shown in Fig. 4a. For both adaptation-to-shape-frequency and adaptation-to-shape-amplitude conditions, we measured *both* SFAEs and SAAEs. For this experiment, the shape-frequency and shape-amplitude ratios at the PSE were calculated as the mean geometric ratio of test to comparison values over the last 20 trials.

We can make two predictions. First, if the two principle axes of a symmetric curve, the sag and cord, are *not* separately adaptable we expect that even if the adaptors differ only in shape-frequency (the adaptation-to-shape-frequency condition) *both* the SFAE and SAAE will be observed. Similarly, even if the adaptors differ only in shape-amplitude (the adaptation-to-shape-amplitude condition) both the SFAE and SAAE will be observed. On the other hand if the sag and cord are independently adaptable we expect that if the adaptors differ only in shape-frequency, *only* the *SFAE* will be observed, and if the adaptors differ only in shape-amplitude, *only* the SAAE will be observed.

Fig. 4 shows (b) SFAEs and (c) SAAEs as a function of adaptor shape-frequency for the adaptation-to-shape-frequency condition (light gray symbols), and as a function of adaptor shape-amplitude for the adaptation-to-shape-amplitude condition (black symbols). First consider the conventional situation in which the dimension to which the subjects were adapted was the same as that to which they were tested (gray symbols in Fig. 4b, black symbols in Fig. 4c). Note the bi-modal-shaped functions that cross zero at, or close to, the point where adaptor and test have the same value (indicated by the black arrow). This replicates our previous findings (Gheorghiu & Kingdom, 2007a), and shows that the after-effects are bi-directional: positive values indicate that lower shape-frequencies (or shape-amplitudes) cause higher shape-frequencies (or shape-amplitudes) to look higher, negative values show that higher shape-frequencies (or shape-amplitudes) cause

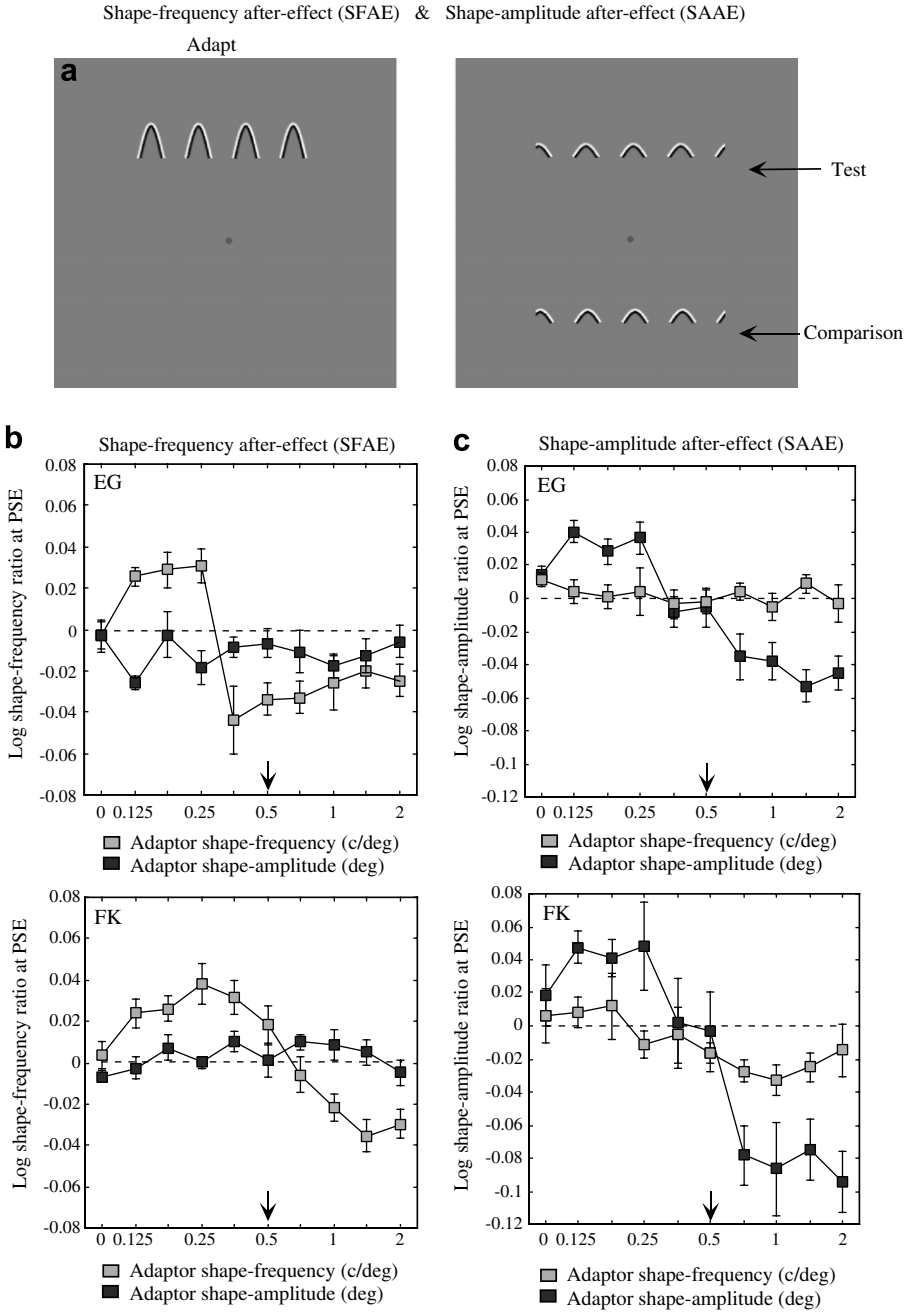

Fig. 4. (a) Example stimuli used in Experiment 3: quasi-half-wave-rectified sinusoidal-shaped contours. (b–c) Results for Experiment 3: (b) SFAEs and (c) SAAEs as a function of adaptor shape-frequency for the adaptation-to-shape-frequency condition (light gray symbols) and as a function of adaptor shape-amplitude for the adaptation-to-shape-amplitude condition (black symbols). The arrow indicates the shape-frequency/amplitude of the test contour.

lower shape-frequencies (or shape-amplitudes) to look lower (light gray symbols in Fig. 4b and black symbols in Fig. 4c).

More pertinent however are the functions in which the adaptor and test dimensions are different (black symbols in Fig. 4b and gray symbols in Fig. 4c). The after-effects in these cases are all close to zero. In other words adaptation to shape-frequency had little or no impact on perceived shape-amplitude, and adaptation to shape-amplitude had little or no effect on perceived shape-frequency. Thus the SFAE and SAAE are independent after-effects. For curves that are ±cosine-shaped, this implies that the sag and the cord are independently adaptable, and therefore encoded as separate dimensions of curvature.

3.4. Experiment 4: Local orientation

Here we examine whether curvature-encoding is selective for local orientation. If curvature-encoding mechanisms are selective for local orientation, we would expect SFAEs and SAAEs to be reduced when the adaptor and

test contours differed in their local orientation content. We used pairs of adaptors and tests that were full sine-wave-shaped contours constructed from odd-symmetric (i.e. d.c. balanced) Gabor patches with a spatial bandwidth of 1.5 octaves and spatial frequency of 5 c/deg (see Fig. 5a). The spacing between the Gabor patches along the contour was 0.4 deg i.e. adaptor and test contours were equally 'sampled' by Gabors. The total number of Gabor patches differed by a factor of 1.48 between the two adaptors, since the length along the contour depends on both its shape-frequency and shape-amplitude for a fixed size window. That is, the adaptor with the high shape-frequency or shape-amplitude was sampled by 34 Gabors, whereas the adaptor with the low shape-frequency or shape-amplitude was sampled by 23 Gabors. The test contour was sampled by 26 Gabors. Example contours are shown in Fig. 5. The orientation of each Gabor patch was (a) either horizontal or vertical, which we refer to as *absolute* orientations (see Fig. 5d–e), or (b) defined in relation to the tangent of the curve, either collinear or orthogonal to it, which we refer to as *relative* orientations (see Fig. 5b–c). There were three relative-orientation conditions: (i) adaptor and test both collinear, C/C; (ii) adaptor and test both orthogonal, O/O, and (iii) adaptor and test of different relative orientation: collinear-adaptor/orthogonal-test and orthogonal-adaptor/collinear-test. Analogous conditions used the absolute orientations: (i) adaptor and test both horizontal, H/H; (ii) adaptor and test both vertical, V/V, and (iii)

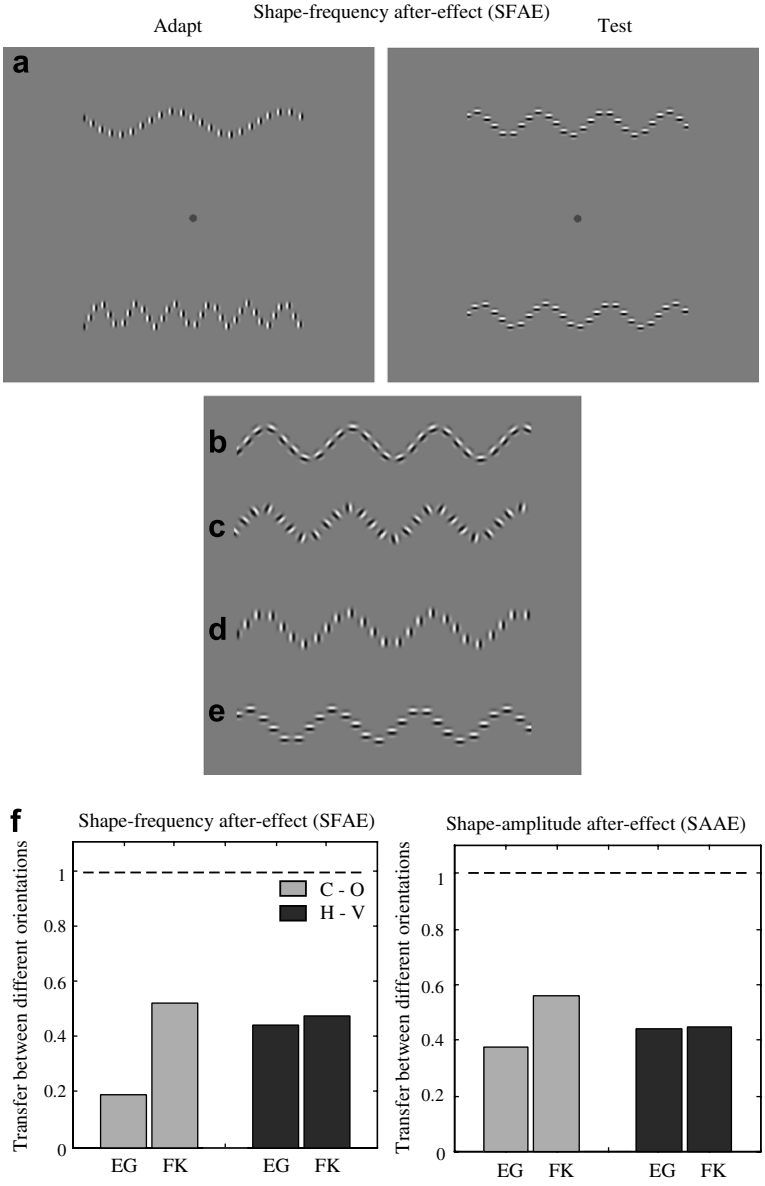

Fig. 5. (a) Example adaptor and test contours used in Experiment 4. The sine-wave-shaped contours were constructed from odd-symmetric (i.e. d.c. balanced) Gabor patches those local orientations are (b) collinear, (c) orthogonal, (d) vertical, and (e) horizontal. (f) Transfer of after-effects between relative orientations (light gray bars) and between absolute orientations (dark gray bars). The value of 1 (dashed-line) indicates complete transfer whereas a value less than 1 indicates partial transfer.

adaptor and test of different local orientation: horizontal-adaptor/vertical-test and vertical-adaptor/horizontal-test.

Fig. 6 shows SFAEs and SAAEs for the relative (Fig. 6a–b) and absolute (Fig. 6c–d) orientation conditions. Same local-orientation adaptors and tests are indicated as white bars and different local-orientation adaptors and tests as gray bars. The dashed lines indicate the size of the after-effects obtained with full sine-wave adaptors and tests. The results show (i) comparable sized after-effects for adaptors/tests with the same local orientation, whether collinear, C/C, orthogonal, O/O, horizontal, H/H, or vertical, V/V (white bars); (ii) comparable sized after-effects for adaptors/tests with the same local orientation (white bars) with those obtained from full sine-wave adaptors/

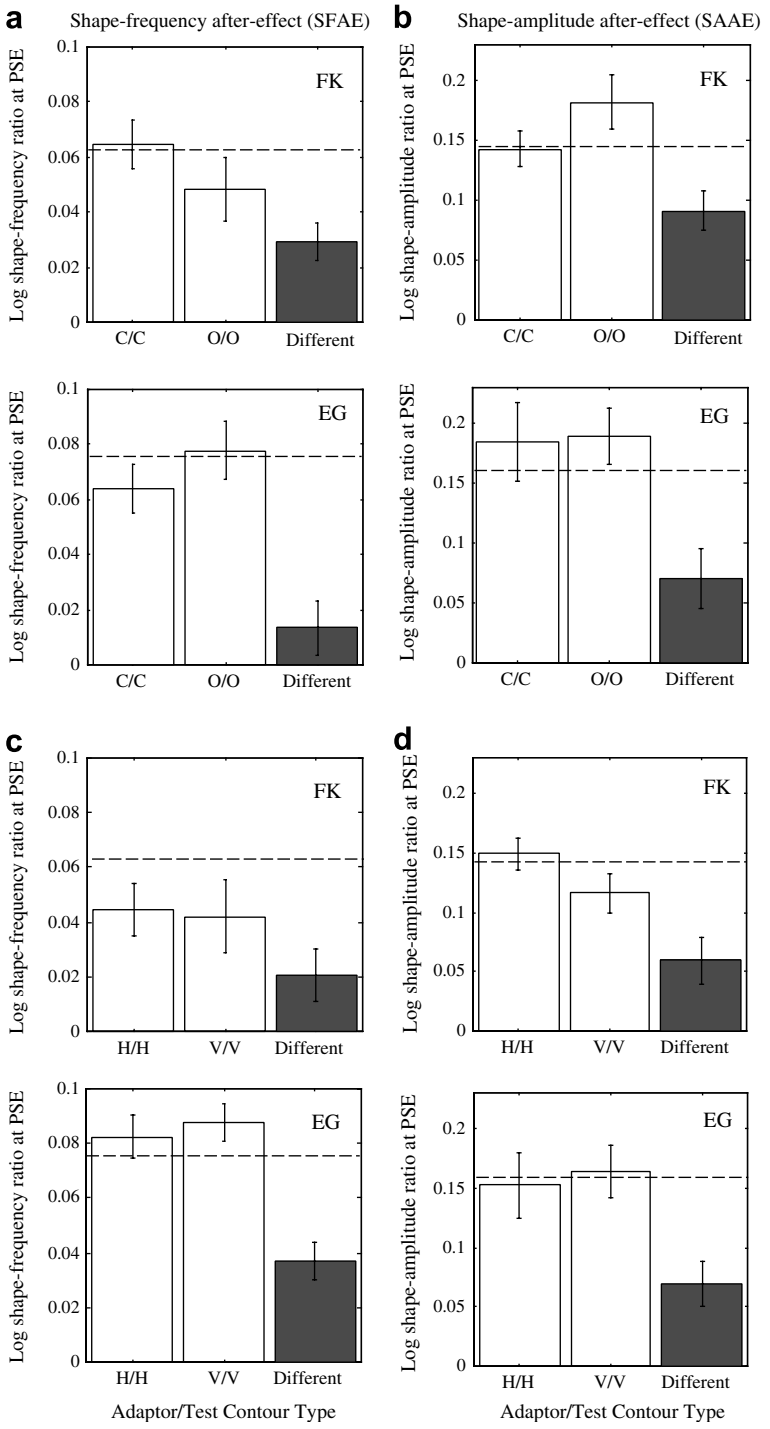

Fig. 6. Results for Experiment 4: (a) SFAEs and (b) SAAEs for same (white bars) and different (gray bars) relative local orientations of Gabor patches: C—collinear, and O—orthogonal. (c) SFAEs and (d) SAAEs for same (white bars) and different (gray bars) absolute local orientations of Gabor patches: H—horizontal, and V—vertical. For example, O/O stands for orthogonal-adaptor/orthogonal-test. The dashed lines indicate the after-effects obtained with full sine-wave adaptors and tests.

tests (dashed lines); (iii) significantly reduced after-effects for adaptors/tests with different local orientations (gray bars), whether relative or absolute.

To test whether the after-effects are significantly larger for same versus different local orientations we performed a two-way ANOVA (analysis of variance) with Orientation (relative vs. absolute) and Combination (same vs. different local orientations) as factors, on both the SFAE and SAAE data (Fig. 6), for each subject. The main effect of Combination was significant [for SFAE: $F(1,1) = 14.68$, $p < 0.05$ for F.K.; $F(1,1) = 293.24$, $p < 0.05$ for E.G.; for SAAE: $F(1,1) = 10.36$, $p < 0.05$ for F.K.; $F(1,1) = 28.01$, $p < 0.05$ for E.G.]. The effect of Orientation was not significant [for SFAE: $F(1,3) = 1.51$, $p > 0.01$ for F.K.; $F(1,3) = 18.28$, $p > 0.01$ for E.G.; for SAAE: $F(1,3) = 0.74$, $p > 0.01$ for F.K.; $F(1,3) = 0.29$, $p > 0.01$ for E.G.]. In addition, we performed a two-way ANOVA to test whether the different local orientations (gray bars in Fig. 6) were significantly different from zero, i.e. from the non-adapted condition. They were significantly different [for SFAE: $F(1,1) = 10.19$, $p < 0.05$ for F.K.; $F(1,1) = 25$, $p < 0.05$ for E.G.; for SAAE: $F(1,1) = 36.05$, $p < 0.05$ for F.K.; $F(1,1) = 55.02$, $p < 0.05$ for E.G.].

In order to compare the reduction in the size of the after-effects between observers, we calculated the magnitude of transfer of after-effect between different local orientations, either relative or absolute, for each observer. The amount of transfer of the after-effect was defined as the after-effect obtained with different local orientations divided by the after-effects obtained with same local-orientations. Fig. 5f shows the transfer of SFAE (left panel) and SAAE (right panel) between different local orientations, either relative (light gray bars) or absolute (dark gray bars). The value of 1 (dashed-line) indicates complete transfer whereas a value less than 1 indicates partial transfer. Fig. 5f shows that (i) both after-effects transfer partially between different local orientations (on average, 41% for SFAE and ~46% for SAAE) and, (ii) there is a similar amount of transfer for relative and absolute orientations. These results indicate that both SFAEs and SAAEs show a significant degree of selectivity for local orientation.

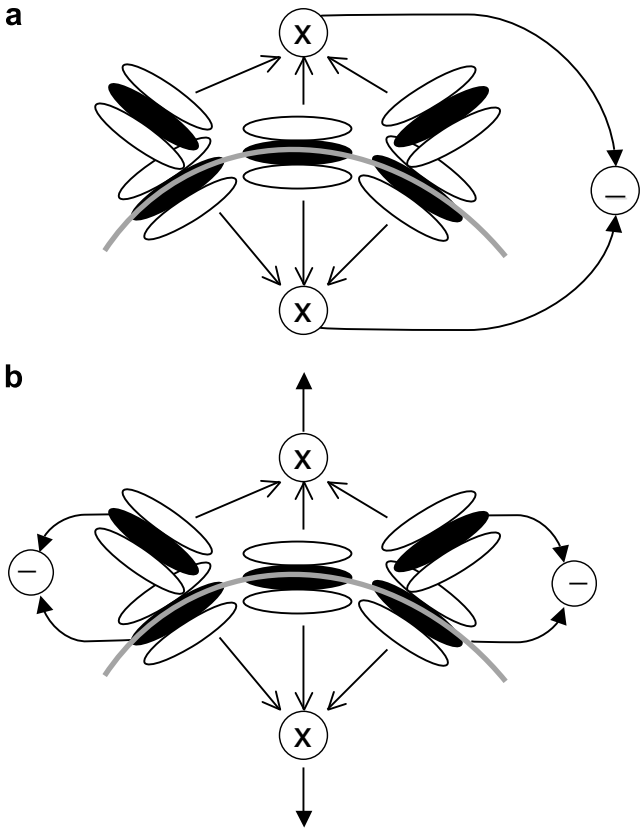

Fig. 7. (a) A schematic representation of Poirier and Wilson (2006) model. Curvature mechanisms are modeled as a multiplicative combination of responses of three oriented filters arranged along a curved path. Curvature opponency takes the form of pairs of mutually inhibitory, opposite-polarity curvature-tuned receptive fields that overlapped at 0/180 cosine phase (for details see Poirier & Wilson, 2006). (b) Our model which shows that curvature receptive fields are not organized in an opponent manner and that 'iso-orientation surround suppression', or IOSS influences the curvature-encoding mechanism.

3.5. Experiment 5: Curvature opponency?

In this experiment we examine whether curvature-encoding mechanisms are arranged in an opponent manner, as recently proposed by Poirier and Wilson (2006). In their model, curvature opponency took the form of pairs of mutually inhibitory, opposite-polarity curvature-selective receptive fields that overlapped at 0/180 cosine phase, as illustrated in Fig. 7a. Here we test experimentally whether or not curvature opponency exists.

In our tests for curvature opponency, we used quasi-half-wave-rectified sinusoidal-shaped adaptors and tests, and potential opponent or inhibitory curves (simply termed inhibitors from now on) that were added to the adaptors (see Fig. 8a). The inhibitors were also quasi-half-wave-rectified sinusoidal-shaped contours with various degrees of curvature, added to each adaptor segment either at its horizontal position, i.e. abutting with it (see Fig. 8b), or at various spatial offsets (Fig. 9a–d).

3.5.1. Experiment 5A: Effect of inhibitor curvature

In the first part of the experiment we examine the effect, if any, of the curvature of the inhibitors. The average unsigned curvature of a sinusoidal contour is proportional to the product of its shape-frequency and shape-amplitude (see Appendix). We used eight values of inhibitor curvature per adaptor, with the constraint that the inhibitors were all equal in contour length to their corresponding adaptors (see Fig. 8a and b). Under this constraint both the shape-frequency and shape-amplitude of the underlying sinusoid had to be co-varied. The resulting curvatures were calculated as the product of shape-frequency and shape-amplitude, which is in units of cycles. Although other measures of curvature exist, such as the mean radius of curvature, the measure used here is intuitively the most appropriate

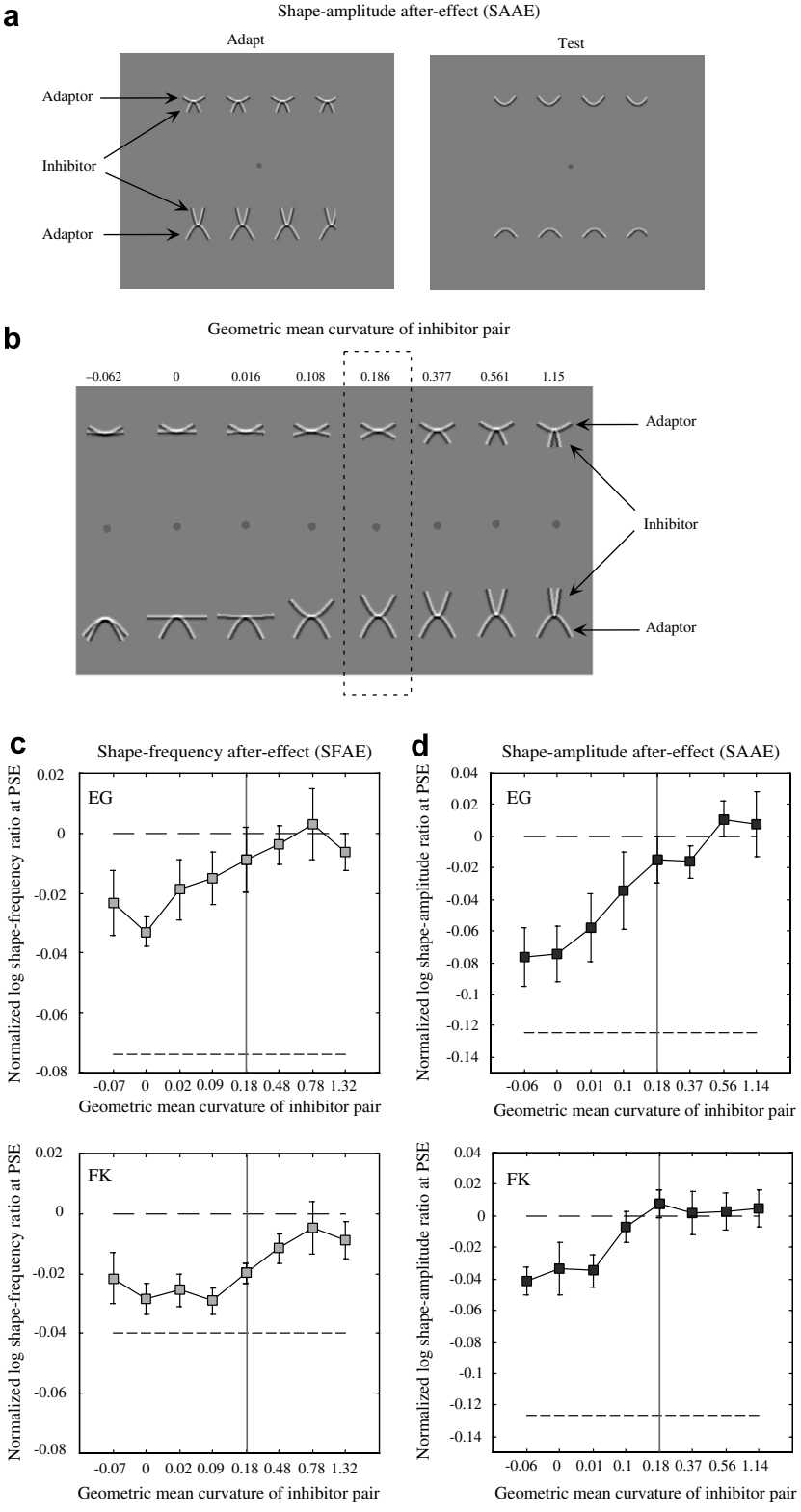

Fig. 8. Experiment 5A: effect of inhibitor curvature. (a) Example quasi-half-wave-rectified sinusoidal-shaped adaptors, inhibitors and test contours. (b) Example of single segments of adaptors and inhibitors for various degrees of inhibitor curvature. The dashed-square indicates adaptor-inhibitor of equal-but-opposite curvatures. (c–d) Results for (c) SFAEs (light gray symbols) and (d) SAAEs (black symbols) normalized to the no-inhibitor values, as functions of geometric-mean inhibitor curvature. The coarse-dashed lines indicate the after-effects obtained in the absence of inhibitors. The fine-dashed lines indicate the no adaptation (and no inhibitors) baselines. The vertical gray lines in (c) and (d) indicate the adaptor-inhibitor of equal-but-opposite curvatures.

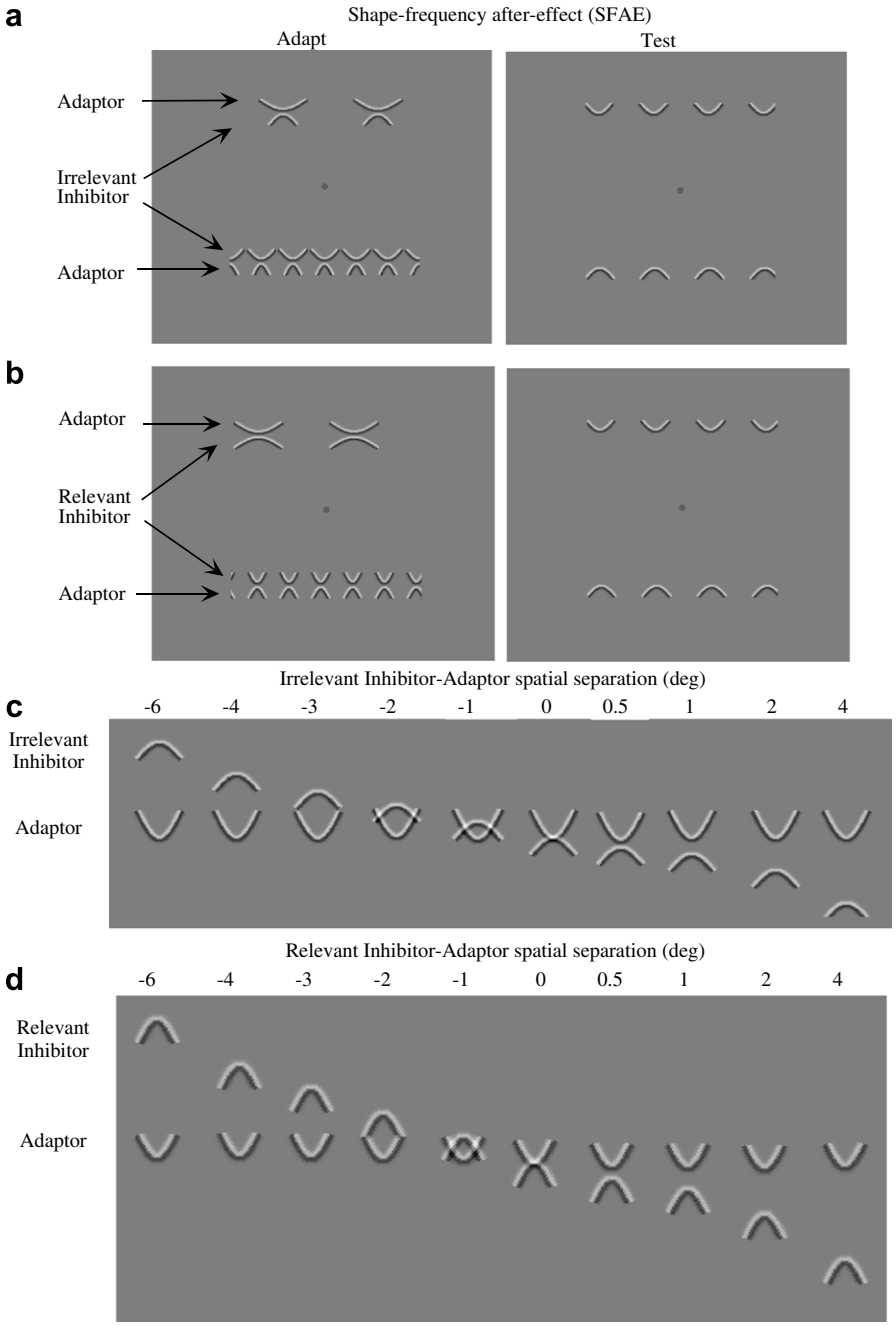

Fig. 9. Experiment 5B: spatial separation. (a) Examples of 'irrelevant' inhibitor, adaptor and test contours. An '*irrelevant*' inhibitor is tied to the shape-frequency and shape-amplitude of the *test* contour, for both adaptors, and therefore unable to contribute towards the after-effects, i.e. inhibitor and test are of equal-but-opposite curvature (compare inhibitor and test). (b) Examples of 'relevant' inhibitor, adaptor and test contours. A '*relevant*' inhibitor is tied to the shape-frequency and shape-amplitude of the *adaptor*, i.e. inhibitor and adaptor are of equal-but-opposite curvature (compare adaptor with the abutting inhibitor). (c–d) Example of single fragments of (c) irrelevant and (d) relevant inhibitors, for various inhibitor-adaptor separations.

given our use of sinusoidal-shaped contours. The inhibitor segments were positioned such that their peaks or troughs overlapped with those of the adaptors, as shown in Fig. 8a and b.

For the SFAE, we used a pair of adaptors with shape-amplitude of 0.43 deg and shape-frequencies 0.25 c/deg and 0.75 c/deg. Because the adaptors were of different shape-frequencies, their cosine-phase half-cycle lengths were different: 4.42 deg and 2.25 deg, respectively. Thus, the contour lengths of the inhibitors were 4.42 deg and 2.25 deg for the two adaptors. For the 0.25 c/deg adaptors, inhibitor curvatures were −0.0498, 0.0, 0.0243, 0.0559, 0.1075, 0.4739, 0.7727 and 1.6260, whereas for the 0.75 c/deg adaptors, inhibitor curvatures were: −0.1189, 0.0, 0.0223, 0.1404, 0.3225, 0.4861, 0.7899 and 1.0832. The geometric mean curvatures of the inhibitor pairs were −0.077, 0.0, 0.023, 0.09, 0.186, 0.48, 0.781 and 1.327, and the geometric mean curvature of the adaptor pair was 0.186.

For the SAAE, the pair of adaptors had a shape-frequency of 0.43 c/deg and shape-amplitudes 0.25 deg and 0.75 deg. Again, because the adaptors were of different shape-amplitudes, their cosine-phase half-cycle lengths were different: 2.57 deg and 3.93 deg, respectively. Thus, the lengths of the inhibitors were 2.57 deg and 3.93 deg for the two adaptors. For the 0.25 deg adaptors, the inhibitor curvatures were −0.02, 0.0, 0.02, 0.0604, 0.1075, 0.276, 0.434 and 0.914, whereas for the 0.75 deg adaptors, inhibitor curvatures were −0.1945, 0.0, 0.0127, 0.1945, 0.3225, 0.515, 0.733 and 1.44. The geometric mean curvatures of the inhibitor pairs were −0.062, 0.0, 0.0158, 0.108, 0.186, 0.377, 0.561 and 1.1469, while the geometric mean curvature of the adaptor pair was 0.186. We also measured the SFAE and SAAE in the absence of inhibitors. Fig. 8b shows single segments of inhibitors and adaptors for various degrees of inhibitor curvature.

If curvature mechanisms are organized in an equal-but-opposite curvature-opponent manner then we would expect a U-shaped function of after-effect versus inhibitor curvature, with the minimum when adaptor and inhibitor have equal-but-opposite curvatures (indicated by the dashed-square in Fig. 8b and gray vertical line in Fig. 8c–d). Fig. 8c shows SFAEs (light gray symbols) and Fig. 8d SAAEs (black symbols) normalized to the no-inhibitor values, as a function of the geometric mean of the two inhibitor curvatures that corresponded to the two adaptors. The coarse-dashed lines indicate the after-effect obtained in the absence of inhibitors, whereas the fine-dashed lines indicate the no adaptation (and no inhibitors) baselines. Both SFAEs and SAAEs increase gradually with increasing curvature of the inhibitor pair. There is no minimum when adaptors and inhibitors have the same curvature (vertical gray line). These results do not support the idea that curvature-sensitive mechanisms are organized into mutually inhibitory, equal-but-opposite curvature detectors, as suggested by Poirier and Wilson (2006).

3.5.2. Experiment 5B: Spatial separation

A possible criticism of the above experiment is that the inhibitor pairs of various curvatures might have made a positive contribution to the after-effect in spite of being opposite in polarity (except in four conditions: 0 and −0.077 curvatures for the SFAE and 0 and −0.062 curvatures for SAAE) to the adaptors and positioned in different vertical locations relative to the tests. In the above experiment, the pair of inhibitors co-varied in both the shape-frequency and shape-amplitude of the underlying waveform. In Experiment 3, we showed that adaptation to shape-frequency had little or no impact on perceived shape-amplitude, and adaptation to shape-amplitude had little or no effect on perceived shape-frequency. Therefore, in Experiment 5A, the shape-frequencies of the inhibitors might have positively contributed towards the SFAE and the shape-amplitudes of the inhibitors might have positively contributed towards the SAAE. This positive contribution towards the after-effects might have cancelled any negative contribution resulting from inhibition.

In order to avoid this potential artifact, we conducted an experiment that employed both 'relevant' and 'irrelevant' inhibitors. The terms relevant and irrelevant refer to their possible adaptive effects on the test pair. A relevant inhibitor is 'tied' to the shape-frequency and shape-amplitude of the adaptor (i.e. has the same curvature as the adaptor but of opposite sign, as indicated in Fig. 9b left and by the dashed-square in Fig. 8a). An irrelevant inhibitor is tied to the shape-frequency and shape-amplitude of the test contour, for both adaptors, and therefore unable to contribute towards the after-effect (compare inhibitor and test in Fig. 9a). Examples of irrelevant and relevant inhibitor, adaptor and test pairs are shown in Fig. 9a–b. In this experiment, rather than varying the curvature of the inhibitors as in Experiment 5A, we fixed inhibitor curvature and varied the adaptor-inhibitor vertical separation.

The irrelevant inhibitor pair consisted of quasi-half-wave-rectified sinusoidal-shaped contours with a shape-frequency of 0.43 c/deg and shape-amplitude of 0.43 deg (the same as the test pair) (see Fig. 9a). The relevant inhibitor pair consisted of quasi-half-wave-rectified sinusoidal-shaped contours with the same shape-frequency and shape-amplitude as the adapting pair (see Fig. 9b). Single fragments of the various inhibitor-adaptor separations are shown in Fig. 9c for the irrelevant, and Fig. 9d for the relevant inhibitors. We used eleven spatial separations: −6, −4, −3, −2, −1, −0.5, 0, 0.5, 1, 2 and 4 deg.

If curvature encoders are organized in an opponent manner, then we would expect a U-shaped function of vertical separation, i.e. a minimum after-effect at zero separation. Fig. 10 shows (a) SFAEs and (b) SAAEs, normalized to the no-inhibitor conditions, as a function of the spatial separation between the inhibitor and adaptor, for irrelevant (black squares) and relevant (gray circles) inhibitors. The coarse-dashed lines at zero indicate the after-effect in the absence of the inhibitor (i.e. adaptor present but no inhibitor), while the fine-dashed lines indicate the after-effects in the absence of any adapting stimulus (i.e. no adaptor and no inhibitor). Error bars in the lower left corner indicate maximum and minimum standard errors. The results show firstly that for both relevant and irrelevant inhibitors, there is a local *maximum* in both after-effects when the adaptor-inhibitor separation is zero (indicated by the vertical gray line). The local maximum obtained for zero spatial separation is close to that obtained in the absence of the inhibitors (coarse-dashed lines). Secondly, for intermediate adaptor-inhibitor separations (both positive and negative separations), the after-effects obtained with the irrelevant inhibitors are in general lower than whose obtained with the relevant inhibitors (compare black squares with gray circles).

Our finding of a local maximum instead of a minimum at zero adaptor-inhibitor spatial separation, in both after-effects and for both relevant and irrelevant adaptors, is not consistent with curvature mechanisms being organized

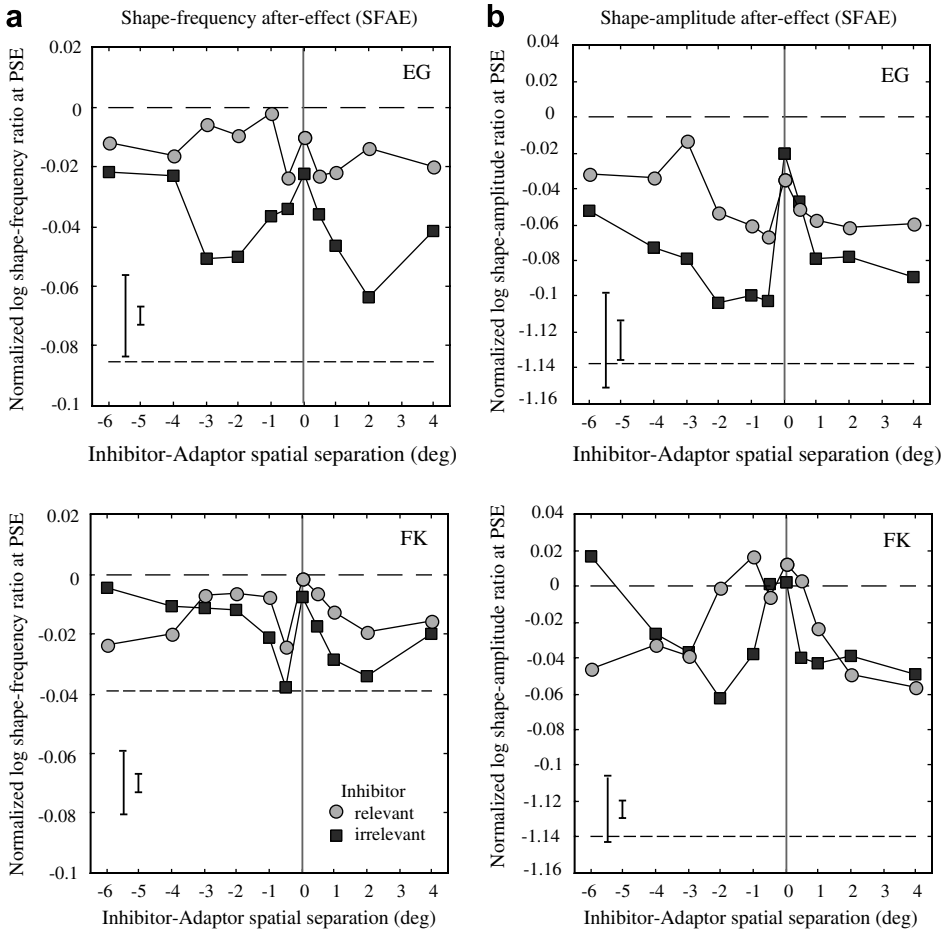

Fig. 10. Experiment 5B: spatial separation. Results: (a) SFAEs and (b) SAAEs, normalized to the no-inhibitor conditions, as a function of the spatial separation between the inhibitor and adaptor, for irrelevant (black squares) and relevant (gray circles) inhibitors. The coarse-dashed lines at zero level indicate the after-effect in the absence of the inhibitor. The fine-dashed lines indicate the no adaptation (and no inhibitors) baselines. Error bars in the lower left corner indicate maximum and minimum standard errors. The vertical gray lines indicate adaptor-inhibitor of 0 deg spatial separation for which Poirier and Wilson (2006) model predicts maximal inhibitory interactions between opponent curvature mechanisms.

in an opponent manner. In the Discussion below we will return to consider why we obtained a local maximum at zero adaptor-inhibitor separation.

4. General discussion

To summarize. SFAEs and SAAEs (i) show a degree of selectivity to adaptor shape-phase; (ii) show a degree of selectivity to curvature polarity or sign; (iii) show a degree of selectivity to local orientation; (iv) are independent after-effects, suggesting that that the two orthogonal axes of a curve, the sag and the cord, are encoded independently; and (v) show no evidence for curvature opponency.

Recently we showed that SFAEs and SAAEs did not result from adaptation to either local orientation or global shape, but instead to local curvature (Gheorghiu & Kingdom, 2007a). The results of the present study have refined our understanding of the spatial properties of curvature-tuned mechanisms. Consider the significance of each finding for our understanding of curvature processing.

1. *Maximum after-effect for 0*/180 deg *shape-phase adaptors*. Gheorghiu and Kingdom (2007a) showed that using full-length sinusoidal adaptors and tests of various sinusoidal lengths, SFAEs and SAAEs reached a maximum when the test was half-a-cycle, provided it was in cosine phase. Sine-phase test fragments reached a maximum when closer to a full cycle. However, only test fragments in cosine and sine phase were tested. In our first experiment (Experiment 1) we used repeating half-cycle adaptors and full-sinusoidal tests, and found the biggest after-effects when the adaptors were in cosine phase. This result reinforces the conclusion that curvature-encoding mechanisms have a mirror-symmetric receptive field structure. Significant after-effects were however obtained with the sine-phase half-cycle adaptors. Why? The reason is probably that a sine-phase half-cycle can be thought of as consisting of two short curves of opposite sign joined together. The two short portions of each half-cycle would presumably still produce some degree of after-effect. The after-effects obtained with quasi-half-wave-rectified adaptors were smaller that those

obtained with full sine-wave adaptors, presumably because the latter have more contrast energy. The size of the after-effect obtained with full sine-wave adaptors was not however a simple sum of those obtained from the various fragmented adaptors, suggesting that adaptations from different parts of the stimuli do not combine linearly.

2. *Selectivity to curvature polarity.* Several studies have shown that curvature polarity is an important feature in shape perception, by reporting an advantage for either positive or negative curvature polarities. For instance, some studies have found an advantage for convexity when judging position (Bertamini, 2001; Bertamini & Mosca, 2004; Loffler, Wilson, & Wilkinson, 2003). Other studies report an advantage for concavities when detecting a change in shape (Barenholtz et al. 2003). To our knowledge however, Experiment 2 is the first psychophysical evidence that curvature mechanisms are selective for curvature polarity.
3. *Selectivity to sag and cord.* Using half-wave rectified sinusoidal shapes, we showed that a wide range of adaptor shape-frequencies had little or no effect on the perceived shape-amplitude of a test, and that a wide range of adaptor shape-amplitudes had little or no effect on the perceived shape-frequency of a test. This indicates that the SFAE and SAAE are largely independent after-effects, in turn suggesting that the sag and cord of a curve are independently processed. Thus curvature might be encoded via two sub-populations of neurons, both selective along a number of dimensions, e.g. luminance polarity, luminance scale, chromaticity, overall orientation, curvature polarity etc., but with one population tuned to curves with various sags and the other tuned to curves with various cords.
4. *Selectivity to local orientation.* Experiment 4 showed that contour-shape encoding mechanisms exhibit some degree of selectivity for absolute local orientation, as well as for local orientation defined in relation to the tangent of the curve. These findings are inconsistent with those of Habak et al. (2004) who considered local orientation selectivity in the context of the detection of radial-frequency patterns. They measured the effects of a radial-frequency mask on the detection of a radial-frequency test, and found that the mask elevated test thresholds by the same amount irrespective of whether the mask orientations were parallel or orthogonal to the curve's tangent. The two most likely reasons for the difference between our results and those of Habak et al. (2004) are that (a) Habak et al. measured shape-detection thresholds whereas we measured shape appearance, and (b) radial-frequency pattern detection is perhaps mediated by mechanisms sensitive to global shape (Wilkinson, Wilson, & Habak, 1998) whereas the after-effects employed here are mediated by mechanisms sensitive to local curvature (Gheorghiu & Kingdom, 2007a).
   Comparable sized after-effects were obtained for adaptors/tests with the same local orientation, whether collinear, orthogonal, horizontal, or vertical, whereas the after-effects were reduced when adaptors and tests differed in local orientation (average transfer ~40%, see Fig. 5f). These results rule out the possibility that curvature encoders are universally non-selective for local orientation. However the significant amount of transfer across local orientation leaves open the possibility that some curvature encoders might be so tuned. The more parsimonious explanation however is that curvature encoders are universally selective for local orientation, but have relatively broad local-orientation tuning.
5. *Absence of curvature opponency*. In Experiment 5 we failed to find any evidence that curvature mechanisms were organized in an opponent manner, as recently proposed by Poirier and Wilson (2006) (see Fig. 7a). One interesting feature of the experiment in which we varied the degree of curvature of the inhibitors (which always abutted the adaptors—see Experiment 5A, Fig. 8a–b) was that the after-effects increased with the absolute difference in curvature between inhibitor and adaptor (Fig. 8c–d). The reason for this is probably the influence of 'iso-orientation surround suppression', or IOSS. This is the effect whereby the presence of surround orientations inhibits the neural response to a test orientation. IOSS is exhibited in some V1 neurons (Blakemore & Tobin, 1972; Cavanaugh, Bair, & Movshon, 1997; Jones, Grieve, Wang, & Sillito, 2001; Knierim & van Essen, 1992; Levitt & Lund, 1997; Nelson & Frost, 1978; Nothdurft, Gallant, & van Essen, 1999; Yao & Li, 2002), and has been demonstrated psychophysically in two ways: first, oriented lines fail to 'pop-out' when surrounded by parallel lines (Petkov & Westenberg, 2003); second, the SFAE is reduced when the adaptor contours are surrounded by parallel contours (Kingdom & Prins, 2005b). Fig. 7b shows a schematic representation of how IOSS might affect curvature-encoding.
   In Experiment 5B, the finding of a local maximum (indicated by the vertical gray line in Fig. 10) instead of minimum when the inhibitors abutted the adaptors is also not consistent with curvature mechanisms being organized in an opponent manner. Furthermore, the finding that for intermediate adaptor-inhibitor separations (both positive and negative separations) the after-effects using the irrelevant inhibitors were in general lower than those using relevant inhibitors (compare black squares with gray circles in Fig. 10), might also reflect a contribution of IOSS. This follows from the fact that the local orientations in the adaptors are more similar to those in the irrelevant than the relevant inhibitors, thus allowing IOSS to manifest itself more strongly with the irrelevant inhibitors.

Could any of these findings be explained in terms of adaptation to local orientation rather than to curvature? Gheorghiu and Kingdom (2007a) showed that local orientation is not the feature underpinning the SFAE and SAAE. They found that comparable sized after-effects were

obtained from sinusoidal- and square-wave-shaped adaptors when using the same, sinusoidal-shaped tests, a fact hard to explain on the basis of orientation adaptation. Additional evidence against local orientation as the adapting feature is the degree of independence of the SFAE and SAAE.

To conclude. In this communication we have examined the spatial properties of curvature-encoding mechanisms. If we include the results of the recent study by Kingdom and Gheorghiu (2007), which provided evidence that the first-stage inputs to curvature detectors are multiplicatively combined (see also Poirier & Wilson, 2006), we can state the following. (1) Curvature is encoded by mechanisms that combine multiplicatively the responses of oriented filters whose receptive fields are arranged in a cosine-shape of given polarity. (2) Some of these mechanisms are selective for the local orientation, and orientation arrangement, of their first-order sub-units. (3) Curvature receptive field shapes have various sags and cords, and these are independently combined to encode perceived sag and cord. (4) Curvature receptive fields are not organized in an opponent manner.

Acknowledgment

This research was supported by a Natural Sciences and Engineering Research Council of Canada (NSERC) Grant # OGP01217130 given to F.K.

Appendix A

Here we provide equations for the various types of contours used.

(i) A full-wave sinusoidal-shaped contour is given by the equation:

$$y(x) = A\sin(2\pi fx + \rho) \quad \text{(AI.1)}$$

where A—shape-amplitude in pixels, f—shape-frequency in cycle per pixels and ρ shape-phase in radians. The average unsigned *curvature* ($\overline{C}$) of a sinusoidal-shaped contour is proportional to the product of its shape-frequency and shape-amplitude: $\overline{C} \propto A \bullet f$.

(ii) A quasi-half-wave-rectified sinusoidal-shaped contour is given by the equation:

$$y(x) = \begin{cases} A\sin(2\pi fx + \rho) & \text{for } \sin(2\pi fx + \rho) > 0 \\ 0 & \text{for } \sin(2\pi fx + \rho) \leqslant 0 \end{cases} \quad \text{(AI.2)}$$

where A, f and ρ are as above. The term 'quasi-half-wave-rectified' refers to the fact that the waveform is missing the part defining the 'd.c.'.

(iii) A quasi-half-wave-rectified sinusoidal-shaped contour with component fragments of a specific phase,

$$y(x) = \begin{cases} A\sin(2\pi fx + \rho + \phi) & \text{for } \sin(2\pi fx + \rho + \phi) > 0 \\ 0 & \text{for } \sin(2\pi fx + \rho + \phi) \leqslant 0 \end{cases} \quad \text{(AI.3)}$$

where A, f, ρ are as above and ϕ is the phase of the component fragments. In Experiment 1, ϕ of the adaptor fragments was set to one of the eight values: 0, $\pi/4$, $\pi/2$, $3\pi/4$,π, $5\pi/4$, $3\pi/2$ and $7\pi/4$.

For each of the above-mentioned type of stimuli, the pixel intensities allocated to each line of pixels are in accordance with the desired luminance profile (see Section 2).

References

Anzai, A., Peng, X., & van Essen, D. C. (2007). Neurons in monkey visual area V2 encode combinations of orientations. *Nature Neuroscience, 10*(10), 11321–13131.

Arguin, M., & Saumier, D. (2000). Conjunction and linear non-separability effects in visual shape encoding. *Vision Research, 40*(22), 3099–3115.

Barenholtz, E., Cohen, E. H., Feldman, J., & Singh, M. (2003). Detection of change in shape: An advantage for concavities. *Cognition, 89*(1), 1–9.

Ben-Shahar, O., & Zucker, S. W. (2004). Sensitivity to curvatures in orientation-based texture segmentation. *Vision Research, 44*(3), 257–277.

Bertamini, M. (2001). The importance of being convex: An advantage for convexity when judging position. *Perception, 30*(11), 1295–1310.

Bertamini, M., & Mosca, F. (2004). Early computation of contour curvature and part structure: Evidence from holes. *Perception, 33*(1), 35–48.

Blakemore, C., & Tobin, E. A. (1972). Lateral inhibition between orientation detectors in the cat's visual cortex. *Experimental Brain Research, 15*, 439–440.

Cavanaugh, J. R., Bair, W., & Movshon, J. A. (1997). Orientation-selective setting of contrast gain by the surrounds of macaque striate cortex neurons. *Neuroscience Abstracts, 23*, 227.

Cohen, E. H., Barenholtz, E., Singh, M., & Feldman, J. (2005). What change detection tells us about the visual representation of shape. *Journal of Vision, 5*(4), 313–321.

Connor, C. E., Brincat, S. L., & Pasupathy, A. (2007). Transformation of shape information in the ventral pathway. *Current Opinion in Neurobiology, 17*, 140–147.

Dobbins, A., Zucker, S. W., & Cynader, M. S. (1987). Endstopping in the visual cortex as a substrate for calculating curvature. *Nature, London, 329*, 438–441.

Dobbins, A., Zucker, S. W., & Cynader, M. S. (1989). Endstopping and curvature. *Vision Research, 29*(10), 1371–1387.

Gallant, J. L., Braun, J., & Van Essen, D. C. (1993). Selectivity for polar, hyperbolic and Cartesian gratings in macaque visual cortex. *Science, 259*(5091), 100–103.

Gallant, J. L., Connor, C. E., Rakshit, S., Lewis, J. W., & Van Essen, D. C. (1996). Neural responses to polar, hyperbolic, and Cartesian gratings in area V4 of the macaque monkey. *Journal of Neurophysiology, 76*(4), 2718–2739.

Gheorghiu, E., & Kingdom, F. A. A. (2006). Luminance-contrast properties of contour-shape processing revealed through the shape-frequency after-effect. *Vision Research, 46*(21), 3603–3615.

Gheorghiu, E., & Kingdom, F. A. A. (2007a). The spatial feature underlying the shape-frequency and shape-amplitude after-effects. *Vision Research, 47*(6), 834–844.

Gheorghiu, E., & Kingdom, F. A. A. (2007b). Chromatic tuning of contour-shape mechanisms revealed through the shape-frequency and shape-amplitude after-effects. *Vision Research, 47*(14), 1935–1949.

Gross, C. G. (1992). Representation of visual stimuli in inferior temporal cortex. *Philosophical Transactions of the Royal Society of London Series B-Biological Sciences 29, 335*(1273), 3–10 [Review].

Habak, C., Wilkinson, F., Zahker, B., & Wilson, H. R. (2004). Curvature population coding for complex shapes in human vision. *Vision Research, 44*, 2815–2823.

Hedge, J., & van Essen, D. C. (2000). Selectivity for complex shapes in primate visual area V2. *Journal of Neuroscience, 20*(5), RC61.

Hoffman, D. D., & Richards, W. A. (1984). Parts of recognition. *Cognition, 18*(1–3), 65–96.

Hubel, D. H., & Wiesel, T. N. (1968). RFs and functional architecture of monkey striate cortex. *Journal of Physiology, 195*, 215–243.

Hulleman, J., te Winkel, W., & Boselie, F. (2000). Concavities as basic features in visual search: Evidence from search asymmetries. *Perception & Psychophysics, 62*(1), 162–174.

Ito, M., Fujita, I., Tamura, H., & Tanaka, K. (1994). Processing of contrast polarity of visual images in inferotemporal cortex of the macaque monkey. *Cerebral Cortex, 4*(5), 499–508.

Jones, H. E., Grieve, K. L., Wang, W., & Sillito, A. M. (2001). Surround suppression in primate V1. *Journal of Neurophysiology, 86*, 2011–2028.

Kayaert, G., Biederman, I., Op de Beeck, H. P., & Vogels, R. (2005). Tuning for shape dimensions in macaque inferior temporal cortex. *European Journal of Neuroscience, 22*(1), 212–224.

Keeble, D. R. T., & Hess, R. F. (1999). Discriminating local continuity in curved figures. *Vision Research, 39*, 3287–3299.

Kingdom, F. A. A., & Gheorghiu, E. (2007). Multiplication of first-stage inputs to curvature detectors. *Journal of Vision, 7*(9), 336.

Kingdom, F. A. A., & Prins, N. (2005a). Different mechanisms encode the shapes of contours and contour-textures. *Journal of Vision, 5*(8), 463.

Kingdom, F. A. A., & Prins, N. (2005b). Separate after-effects for the shapes of contours and textures made from contours. *Perception, 34*(Suppl.), 92 [Abstract].

Knierim, J. J., & van Essen, D. C. (1992). Neuronal responses to static texture patterns in area V1 of the alert macaque monkey. *Journal of Neurophysiology, 67*, 961–980.

Koenderink, J. J., & Richards, W. (1988). Two-dimensional curvature operators. *Journal of the Optical Society of America A, 5*, 1136–1141.

Koenderink, J. J., & van Doorn, A. J. (1982). The shape of smooth objects and the way contours end. *Perception, 11*(2), 129–137.

Koenderink, J. J., & van Doorn, A. J. (1987). Representation of local geometry in the visual system. *Biological Cybernetics, 55*(6), 367–375.

Kramer, D., & Fahle, M. (1996). A simple mechanism for detecting low curvatures. *Vision Research, 36*(10), 1411–1419.

Levi, D. M., & Klein, S. A. (2000). Seeing circles: What limits shape perception? *Vision Research, 40*(17), 2329–2339.

Levitt, J. B., & Lund, J. S. (1997). Contrast dependence of contextual effects in primate visual cortex. *Nature, 387*, 73–76.

Loffler, G., Wilson, H. R., & Wilkinson, F. (2003). Local and global contributions to shape discrimination. *Vision Research, 43*, 519–530.

Missal, M., Vogels, R., Li, C. Y., & Orban, G. A. (1999). Shape interactions in macaque inferior temporal neurons. *Journal of Neurophysiology, 82*(1), 131–142.

Murray, S. O., Kersten, D., Olshausen, B. A., Schrater, P., & Woods, D. L. (2002). Shape perception reduces activity in human primary visual cortex. *Proc. Natl. Acad. Sci. USA, 99*(23), 15164–15169.

Nelson, J. I., & Frost, B. J. (1978). Orientation-selective inhibition from outside the classic receptive field. *Brain Research, 139*, 359–365.

Nothdurft, H. C., Gallant, J. L., & van Essen, D. C. (1999). Response modulation by texture surround in primate area V1: Correlates of "popout" under anesthesia. *Visual Neuroscience, 16*, 15–34.

Op de Beeck, H., Wagemans, J., & Vogels, R. (2001). Inferotemporal neurons represent low-dimensional configurations of parameterized shapes. *Nature Neuroscience, 4*, 1244–1252.

Pasupathy, A., & Connor, C. E. (1999). Responses to contour features in macaque area V4. *Journal of Neurophysiology, 82*(5), 2490–2502.

Pasupathy, A., & Connor, C. E. (2001). Shape representation in area V4: Position-specific tuning for boundary conformation. *Journal of Neurophysiology, 86*(5), 2505–2519.

Pasupathy, A., & Connor, C. E. (2002). Population coding of shape in area V4. *Nature Neuroscience, 5*(12), 1332–1338.

Petkov, N., & Westenberg, M. A. (2003). Suppression of contour perception by band-limited noise and its relation to non-classical receptive field inhibition. *Biological Cybernetics, 88*, 236–246.

Poirier, F. J., & Wilson, H. R. (2006). A biological plausible model of human radial frequency perception. *Vision Research, 46*(15), 2443–2455.

Prins, N., Kingdom, F. A. A., & Hayes, A. (2007). Detecting low shape-frequencies in smooth and jagged contours. *Vision Research, 47*(18), 2390–2402.

Regan, D., & Hamstra, S. J. (1992). Shape discrimination and the judgment of perfect symmetry: Dissociation of shape from size. *Vision Research, 32*(10), 1845–1864.

Roach, N., Webb, B., & Mcgraw, P. (2007). Prolonged exposure to global structure induces 'remote' tilt-aftereffects. *Journal of Vision, 7*(9), 304.

Suzuki, S., & Cavanagh, P. (1998). A shape-contrast effect for briely presented stimuli. *Journal of Experimental Psychology: Human Perception and Performance, 24*(5), 1315–1341.

Tanaka, K. (1996). Inferotemporal cortex and object vision. *Annual Review Neuroscience, 19*, 109–139.

Tyler, C. W. (1973). Periodic vernier acuity. *Journal of Physiology, 228*(3), 637–647.

Watt, R. J., & Andrews, D. P. (1982). Contour curvature analysis: Hyperacuities in the discrimination of detailed shape. *Vision Research, 22*(4), 449–460.

Whittaker, D., & McGraw, P. V. (1998). Geometric representation of the mechanisms underlying human curvature detection. *Vision Research, 38*(24), 3843–3848.

Wilkinson, F., James, T. W., Wilson, H. R., Gati, J. S., Menon, R. S., & Goodale, M. A. (2000). An fMRI study of the selective activation of human extrastriate form vision areas by radial and concentric gratings. *Current Biology, 10*, 1455–1458.

Wilkinson, F., Wilson, H. R., & Habak, C. (1998). Detection and recognition of radial-frequency patterns. *Vision Research, 38*, 3555–3568.

Wilson, H. R. (1985). Discrimination of contour curvature: Data and theory. *Journal of the Optical Society of America A, 2*(7), 1191–1199.

Wilson, H. R. (1991). Pattern discrimination, visual filters and spatial sampling irregularity. In M. S. Landy & J. A. Movshon (Eds.), *Computational models of visual processing*. Cambridge, MA: MIT Press.

Wilson, H. R., & Richards, W. A. (1989). Mechanisms of contour curvature discrimination. *Journal of the Optical Society of America A, 6*, 106–115.

Wilson, H. R., & Richards, W. A. (1992). Curvature and separation discrimination at texture boundaries. *Journal of the Optical Society of America A, 9*(10), 1653–1662.

Xu, Y., & Singh, M. (2002). Early computation of part structure: Evidence from visual search. *Perception & Psychophysics, 64*(7), 1039–1054.

Yao, H., & Li, C.-Y. (2002). Clustered organization of neurons with similar extra-receptive field properties in the primary visual cortex. *Neuron, 35*, 547–553.

Zetzsche, C., & Barth, E. (1990). Fundamental limits of linear filters in the visual processing of two-dimensional signals. *Vision Research, 30*(7), 1111–1117.